

# Optimization of Power-Amplifier Load Impedance and Waveform Bandwidth for Real-Time Reconfigurable Radar

MATTHEW FELLOWS, Student Member, IEEE  
MATTHEW FLACHSBART, Student Member, IEEE  
JENNIFER BARLOW, Student Member, IEEE  
JOSEPH BARKATE, Student Member, IEEE  
CHARLES BAYLIS, Member, IEEE  
LAWRENCE COHEN, Senior Member, IEEE  
ROBERT J. MARKS II, Fellow, IEEE  
Baylor University  
Waco, TX, USA

**To create a reconfigurable radar transmitter, the power amplifier circuitry and waveform must be able to adjust in real time to changing operating frequencies and spectral requirements. For range radars, better range resolution can be accomplished by using waveforms of higher bandwidth. In this case it is desirable to maximize the chirp waveform bandwidth while maintaining spectral compliance and meeting power-added efficiency requirements. Based on the concept of the Smith Tube (presented in a recent conference article), this article describes a new intelligent, vector-based search for the load impedance and waveform bandwidth. The search provides the largest possible bandwidth while maintaining the power-added efficiency and adjacent-channel power ratio within specified requirements. The algorithm is demonstrated in measurement with multiple starting impedances and bandwidth search ranges, and consistently accurate and useful results are obtained. Multiple iterations of the two-part search can be performed for increased precision if the time needed to take additional measurements can be tolerated.**

Manuscript received May 15, 2014; revised September 8, 2014, November 25, 2014; released for publication February 4, 2015.

DOI. No. 10.1109/TAES.2015.140381.

Refereeing of this contribution was handled by F. Gini.

This work has been funded under a grant from the National Science Foundation (Award Number ECCS-1343316) to Baylor University.

Authors' address: Baylor University, Electrical and Computer Engineering, One Bear Place 97356, Waco, TX 76798-7356, E-mail: (Charles\_Baylis@Baylor.edu)

0018-9251/15/\$26.00 © 2015 IEEE

## I. INTRODUCTION

The increasing demands on radar systems to perform their needed civilian and military applications are prompting radar engineers to search for new solutions. A radar system must maintain its detection capability while operating efficiently and meeting spectral requirements. To be compatible with a possible future dynamic-spectrum access environment, future radar systems may need to be capable of real-time reconfiguration to change operating frequency and adjust to different spectral output requirements. Measurement-based algorithms to allow fast reconfiguration will be valuable in the development of real-time reconfigurable radar systems.

The bandwidth of a radar waveform is significant in determining the radar range resolution. Therefore, a fundamental conflict in radar design is the trade-off between low-ambiguity range estimation and abiding within ever more stringent spectral requirements. In this article, we demonstrate how a radar chirp waveform's bandwidth can be maximized while meeting imposed limitations on adjacent-channel power and power efficiency.

In our previous work, we have presented load-impedance optimizations to maximize the power-added efficiency (PAE) while meeting requirements on the adjacent-channel power ratio (ACPR) of a transmitter for a fixed-bandwidth waveform [1]. The well-known equation for the PAE is

$$\text{PAE} = \frac{P_{\text{out,RF}} - P_{\text{in,RF}}}{P_{\text{DC}}} \times 100\%, \quad (1)$$

where  $P_{\text{out,RF}}$  is the radio-frequency output power,  $P_{\text{in,RF}}$  is the radio-frequency input power, and  $P_{\text{DC}}$  is the DC power (all in watts). The ACPR is simply the ratio of the total measured power in a defined adjacent channel to the total measured power in the defined main channel. Both PAE and ACPR are significantly dependent upon the load impedance [2, 3]. In a recent article [4], we presented the Smith Tube as a cylindrical extension of the Smith chart with chirp waveform bandwidth plotted along the axis of the cylinder. That article shows how premeasured power-amplifier load-pull data taken at multiple bandwidths can be used to select an optimum combination of load impedance and bandwidth to maximize the bandwidth of the transmitted waveform, while maintaining PAE and ACPR requirements.

ACPR results for amplifier broadband signal excitations have been connected with third- and fifth-order intermodulation [5]. Sechi describes in his work how to design load impedance for third-order intermodulation distortion and power from premeasured load-pull data using a graphical technique [6]. This relates to the present article because compromise between two objectives is considered; however, premeasured data are used rather than an efficient measurement-based search algorithm. Sun and Lau have demonstrated the use of genetic algorithms for antenna impedance tuning [7, 8], and the

literature also presents approaches such as fuzzy control [9], neural networks [10], and least-squares optimization [11] for real-time impedance tuning. Sun et al. suggest reconfigurable matching networks as a tool for providing high-efficiency transmitters [12]. Kingsley and Guerci demonstrate an adaptive amplifier module capable of adjusting to optimize for different requirements, such as PAE, minimization of third-order intermodulation, and output power [13]. This previous work demonstrates that the technology and ability to integrate adaptive circuit techniques are available; the present article provides intelligent algorithms that allow such optimizations to be performed quickly and integrated with optimization of the waveform.

Optimization of the radar waveform separate from the circuit optimization has been thoroughly discussed in the radar literature, but the present article presents (to our knowledge) the most profound effort at optimizing the circuit and waveform simultaneously. Simultaneous optimization of transmitter amplifier circuit and waveform will be necessary to meet the demands of next-generation radar. A paradigm of radar systems known as adaptive radar is under development that will be able to adjust its design in real time for differing detection requirements, hopping in frequencies and meeting dynamically changing spectrum requirements. Adaptive-radar techniques will be useful, among other applications, in cognitive radar systems, where a radar learns about and responds to its environment [14, 15]. The design of spectrally confined waveforms through variable-modulus techniques is described in [16]; constant-modulus techniques are also often used for the purpose of maximizing the efficiency of the system. Constant-modulus techniques include continuous-phase modulation [17, 18] and piecewise linear chirp optimization [19, 20]. Optimization of the waveform for a target ambiguity function has been performed by Patton [21], Holtzman and Thorp [22], Wong and Chung [23], and Sussman [24]. Guerci and Pillai suggest the need for radar waveform optimization to take into account the transmitter, receiver, and channel [25]. Waveform optimization for detection and estimation in cognitive radio is described by Haykin et al. [26]. Goodman et al. describe adaptive waveform design using matched illumination and sequential hypothesis testing to efficiently detect targets [27]. The present article describes maximization of the waveform bandwidth, which is a factor in providing range resolution capability.

The idea for a joint optimization is a logical next step based on the work of Jakobosky et al., who explore the effect of an “amplifier in the loop” on the waveform’s ambiguity function, concluding that distortion due to amplifier nonlinearities results in increased range side lobes [28]. Microwave-circuit designers have for some time attempted to compensate for circuit nonlinearities by adjusting the input waveform through a method known as predistortion [29]. Our approach attempts to jointly optimize the waveform with the circuit instead, whereas

predistortion is focused on reducing the impact of nonlinearities on the waveform (more like the “amplifier in the loop” problem). By jointly optimizing the circuit and waveform, we expect the optimal solution will result, providing advances over a simple circuit or waveform optimization.

The Smith Tube, which we recently presented in [4], is a unique extension of the Smith chart to provide an optimization space for a variable-bandwidth chirp and the load reflection coefficient  $\Gamma_L$ . While this extension of the Smith chart is unique, other extensions of the Smith chart in the literature include the spherical extension by Zelley for mapping negative real impedances [30], also assisted by the work of Wu et al. [31]. Shamim et al. have generalized the Smith chart to include fractional circuit elements [32]. Kretzschmar and Schoonaert describe a Smith-chart modification for lossy transmission lines [33]. However, the Smith Tube is the first extension of the Smith chart known to the present authors for joint circuit and waveform optimization.

The limitation of the premeasured load-pull selection approach we presented in [4] is that a load pull of the entire Smith chart at multiple bandwidths often requires hours (as it did for the measurements in that article). This is obviously not feasible in a real-time, reconfigurable radar unless premeasured data are available for all conditions available to the transmitter. The present article shows how an intelligent, measurement-based search can be performed within the Smith Tube to find the optimum combination of load impedance and bandwidth with a small number (20 to 30) of measured load-impedance/bandwidth combinations. This will provide the speed necessary for a radar transmitter to quickly reconfigure to a new operating frequency and changing spectral conditions.

The surface containing combinations of  $\Gamma_L$  and  $B$  providing constant PAE—the PAE surface—is expected to be convex or near convex. The literature shows that the nonlinear output power contours can be generated exactly if an output model for the device parasitics is known [34]. Because input power is fixed for this optimization, the PAE is largely dependent on the contours of output power, which are convex in the Smith chart. While expected to be convex in the two-dimensional Smith chart, the PAE surface is not necessarily convex within the three-dimensional space of the Smith Tube, as our measurements demonstrate.

The ACPR is not expected to be convex in the Smith chart, based upon the literature, although its observed behavior for most devices shows that undesirable local optima will likely be significant distances from the global optima in the Smith chart. An example of load-pull contours demonstrated in the literature for a similar linearity metric (intermodulation rejection) is shown by Hajji et al. [35]. Because a constraint is placed on the PAE in the optimization, and the PAE optimum is normally close to the ACPR optimum, this will tend to force the optimization toward the global ACPR optimum.

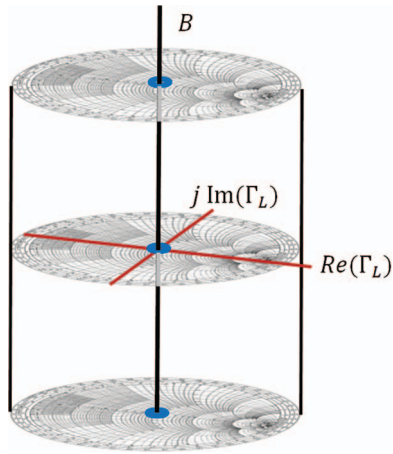


Fig. 1. Smith Tube. Vertical axis represents bandwidth of input chirp waveform, while horizontal cross section of tube is conventional Smith chart [4].

The contribution of this article is the demonstration of an algorithm to jointly optimize the input waveform bandwidth and load impedance to maximize bandwidth while meeting constraints on the PAE and ACPR. Section II describes the Smith Tube, a three-dimensional extension of the Smith chart which will be used as the optimization space. Section III presents the two-part search algorithm, and Section IV presents the measurement results from the algorithm testing. Section V presents some conclusions resulting from this work.

## II. THE SMITH TUBE FOR CIRCUIT AND WAVEFORM OPTIMIZATION

The Smith Tube, first presented in [4], is useful for the optimization of bandwidth  $B$  under PAE and ACPR constraints. The Smith Tube is shown in Fig. 1. The plane is a conventional Smith chart containing all passive values of amplifier load reflection coefficient  $\Gamma_L$  (each mapping to a load impedance  $Z_L$ ). A well-known equation relating reflection coefficient  $\Gamma_L$  to load impedance  $Z_L$  is

$$\Gamma_L = \frac{Z_L - Z_0}{Z_L + Z_0}, \quad (2)$$

where  $Z_0$  is the reference impedance [36]. As the impedance is frequency dependent, the value of  $\Gamma_L$  is also frequency dependent. The value of  $\Gamma_L$  at the center frequency of the band is used for the optimization.

The vertical axis represents the waveform bandwidth  $B$ . In this case,  $B$  represents the difference between the start and stop frequencies of the chirp waveform's frequency sweep (this may or may not correspond to the measurement bandwidth as defined by other standards). As presented in [4], the design objective is to operate in the Smith Tube at the highest intersection point of the surfaces representing acceptable PAE and ACPR values, as shown in Fig. 2. This allows selection of the maximum chirp bandwidth that allows the power amplifier to meet PAE and ACPR requirements.

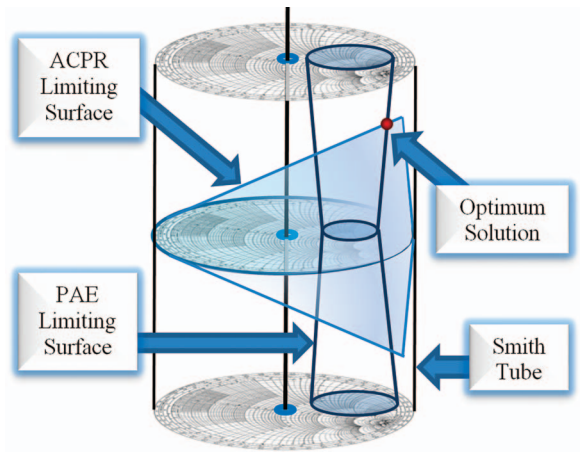


Fig. 2. Conceptual drawing of Smith Tube containing example surfaces for limiting PAE and ACPR values. Optimum point is selected as highest point of intersection (representing largest bandwidth) between surfaces representing limiting PAE and ACPR values [4].

As shown in Fig. 2, it is expected that the enclosing values of  $\Gamma_L$  that give acceptable ACPR will decrease in width as the bandwidth is increased, because more of the unwanted intermodulation distortion spills into the adjacent channel for excitation waveforms with larger bandwidth. It is also expected that the PAE will be nearly constant with increasing bandwidth, because the PAE is calculated from an output power measurement performed with a broadband power sensor. Slight variation may be encountered with changing bandwidth, due to the slight variation of the load impedance with frequency over the bandwidth of the waveform.

## III. SEARCH ALGORITHM

We present a search algorithm to find the optimum location in the Smith Tube, defined as the point providing the largest bandwidth  $B$ . The algorithm proceeds as a two-part search, first employing a vector-based search for  $\Gamma_L$  at a fixed bandwidth  $B$  at the center of the user-defined bandwidth search interval (similar to the load-pull algorithm we described in [1]), then holding the value of  $\Gamma_L$  constant while increasing the bandwidth. The search in [1] triangulates within the Smith chart only and does not include bandwidth considerations; the search in the present article uses an adaptation of the search in [1] as Part A, then performs an optimization for bandwidth as Part B. The new two-part search can be repeated as desired to improve the precision of the solution. A conceptual diagram of the search is sketched in Fig. 3. The details follow.

The user inputs an initial starting value for load reflection coefficient  $\Gamma_L$  and upper and lower search limits for the bandwidth  $B$ . The user also enters the PAE and ACPR limits, as well as the bandwidth resolution parameter  $B_{stop}$ , which represents the minimum interval size for the interval halving that will be performed in the bandwidth part of the search, and the  $\Gamma_L$  "neighboring-point distance" resolution parameter  $D_n$ ,

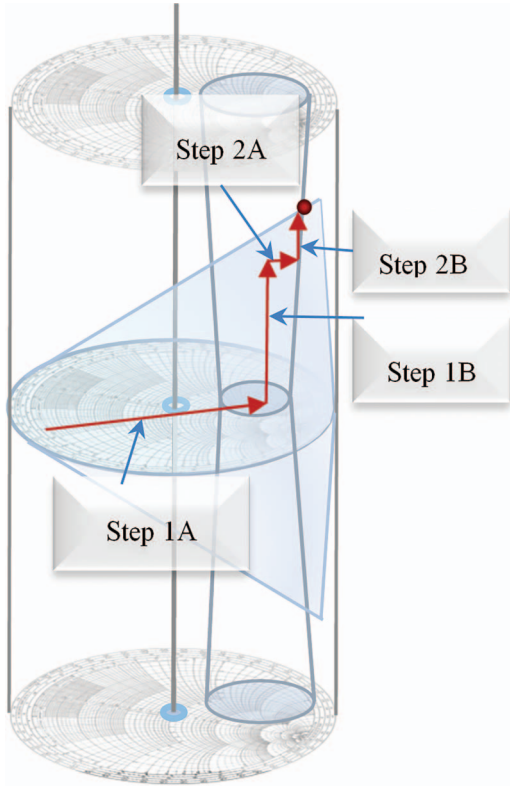


Fig. 3. Search algorithm path for two-part fast search to maximize chirp waveform bandwidth while meeting PAE and ACPR requirements.

which is the distance from the candidate point to measurement points taken for approximation of the gradients [1]. The user also enters the value for  $D_s$ , the search distance parameter that appears in the equations defining the search components. The values of  $D_n$  and  $D_s$  are in reflection-coefficient units, so a value of 1 for either of these parameters is equal to the radius of the Smith chart. A typical value for  $D_s$  in our searches is 0.5, and typical values for  $D_n$  are 0.05 or 0.1 for “uneducated” searches. For searches where the user knows the approximate vicinity of the solution and can start closer to the optimum, a smaller value of  $D_s$  can be entered. Part A and Part B of the search are now described in detail.

#### A. Search for Reflection Coefficient

The search for the optimum  $\Gamma_L$  in the plane proceeds in a similar fashion to the search described in [1], but reversing the roles of PAE and ACPR. At the initial candidate and all subsequent candidate values of  $\Gamma_L$ , the gradients are estimated by measurement of two surrounding  $\Gamma_L$  values in the Smith-chart plane, as shown in Fig. 4. One point is separated to the right of the candidate  $\Gamma_L$  by a small distance  $D_n$ , and the other is separated above the candidate  $\Gamma_L$  by distance  $D_n$  in the Smith-chart plane. PAE and ACPR measurements are taken for these values of  $\Gamma_L$  and used to estimate the PAE and ACPR gradients.

Fig. 5 shows the construction of the search vector to identify the next candidate  $\Gamma_L$  in Part A of the search. This

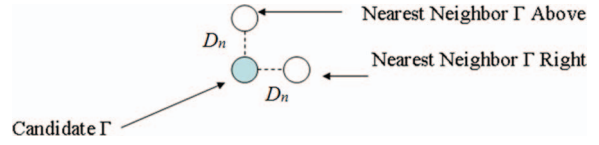


Fig. 4. Measurement of surrounding values of  $\Gamma_L$  in Smith-chart plane for PAE and ACPR gradient estimation at candidate  $\Gamma_L$ .

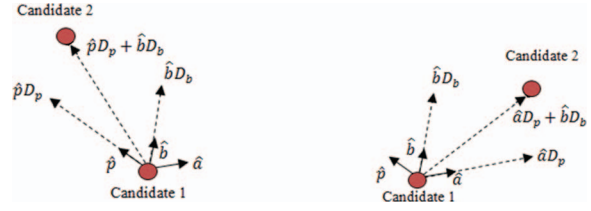


Fig. 5. Graphical description of Smith-chart step vectors in determination of new candidate point for cases when (a) PAE at Candidate 1 is less than specified minimum (unacceptable) and (b) PAE at Candidate 1 is greater than specified minimum (acceptable).

part of the search is performed with the bandwidth  $B$  fixed at the center of the user-specified bandwidth search range. Proceeding from the first (and any subsequent) given candidate value for  $\Gamma_L$ , the subsequent value of  $\Gamma_L$  to be examined in the search is found by adding the vector

$$\bar{v} = \hat{p}D_p + \hat{b}D_b \quad (3)$$

to the present candidate value of  $\Gamma_L$ . The unit vector  $\hat{p}$  is in the direction of steepest PAE ascent (in the estimated PAE gradient direction), and the unit vector  $\hat{b}$  is in the direction of the bisector between the PAE gradient and the negative of the ACPR gradient. This vector has two components: The component  $\hat{p}D_p$  points the search toward the PAE optimum, and the component  $\hat{b}D_b$  points the search toward the locus of Pareto optimum solutions (the constrained optima for ACPR under different PAE limitations). Because the gradients for ACPR and PAE will be collinear on the Pareto optimum locus, the unit vector  $\hat{b}$  bisecting  $\hat{a}$  and  $\hat{p}$  tends to point toward a minimum path to get to the Pareto optimum locus. This allows the search to proceed directly toward the constrained optimum. The values of  $D_p$  and  $D_b$  are the values of the search-vector components in these directions, and are computed as follows:

$$D_p = \frac{D_s}{2} \frac{|\text{PAE}_{\text{meas}} - \text{PAE}_{\text{target}}|}{|\text{PAE}_{\text{worst}} - \text{PAE}_{\text{target}}|} \quad (4)$$

$$D_b = \frac{D_s}{2} \frac{|\theta_{\text{meas}} - \theta_{\text{target}}|}{\theta_{\text{target}}} \quad (5)$$

The value  $\text{PAE}_{\text{worst}}$  is the lowest value of PAE measured, while  $\text{PAE}_{\text{target}}$  is the minimum acceptable PAE. The angle  $\theta_{\text{target}}$  is the target angle between  $\hat{p}$  and  $\hat{b}$  in Fig. 5, and its value is  $90^\circ$ , because  $\hat{p}$  and  $\hat{a}$  are collinear on the Pareto optimum locus (the ACPR and PAE contours are tangent to one another on the Pareto optimum locus) and the desired solution to the constrained optimization at

hand lies on the Pareto optimum locus [37].  $\text{PAE}_{\text{meas}}$  and  $\theta_{\text{meas}}$  are the measured value of PAE and the angle between  $\hat{p}$  and  $\hat{b}$ , respectively. The preceding description is for the case where the initial candidate is in a region of the Smith chart where the PAE value is smaller than the minimum acceptable value  $\text{PAE}_{\text{target}}$ . Both (4) and (5) serve as estimates of the percentage of progress from the worst-case value to the goal in terms of obtaining desired  $\text{PAE}-D_p$  in (4)—and reaching the Pareto front— $D_b$  in (5). If instead the PAE is acceptable at the present candidate value (greater than  $\text{PAE}_{\text{target}}$ ), then the vector to the next candidate is given by

$$\bar{v} = \hat{a}D_p + \hat{b}D_b, \quad (6)$$

where  $\hat{a}$ , the unit vector in the direction opposite to the ACPR gradient, is used instead of  $\hat{p}$ .

Part A of the search ends when the magnitude of the search vector  $\bar{v}$  is less than  $D_n$ .

### B. Search for Bandwidth

After the Part A search for the value of  $\Gamma_L$  providing the smallest value of ACPR while keeping PAE above a specific minimum,  $\Gamma_L$  is held constant at the Part A optimum while the bandwidth  $B$  is adjusted. If Part A of the search results in an ACPR value within the ACPR requirements, this means that the bandwidth needs to be increased to reach the highest point of intersection between the PAE and ACPR surfaces: the optimum solution. If Part A of the search results in a minimum ACPR value that is larger than the maximum allowable ACPR, then the bandwidth needs to be reduced in Part B of the search to allow lower values of ACPR to be obtained while meeting PAE requirements.

Interval halving is used for the process of vertical searching in the Smith Tube. A range of candidate chirp bandwidth values is specified by the user for the bandwidth optimization. Part A of the search involves the optimization of ACPR under a PAE constraint at the center bandwidth of the range. If the ACPR value resulting from Part A is within constraints, the bandwidth is increased again to halve the interval between this bandwidth and the upper bandwidth limit. If the ACPR value resulting from Part A is not within constraints, the bandwidth interval is halved between the starting bandwidth and the lower bandwidth limit. Interval halving is performed repeatedly in this way until the half-interval size for search step decreases below a selected limiting resolution value  $B_{\text{stop}}$ . At this point, the combination of the largest successful measured value of  $B$  (the highest value of  $B$  providing ACPR and PAE within the specified limits) and the accompanying result of Part A for  $\Gamma_L$  is chosen as the optimum ( $B, \Gamma_L$ ) combination.

Following the completion of Part B, it is possible (and in some cases encouraged) to repeat both Parts A and B, beginning from the combination of  $\Gamma_L$  and  $B$  resulting from the first iteration. This takes into account the possible change in PAE with  $B$  (often expected to be a slight

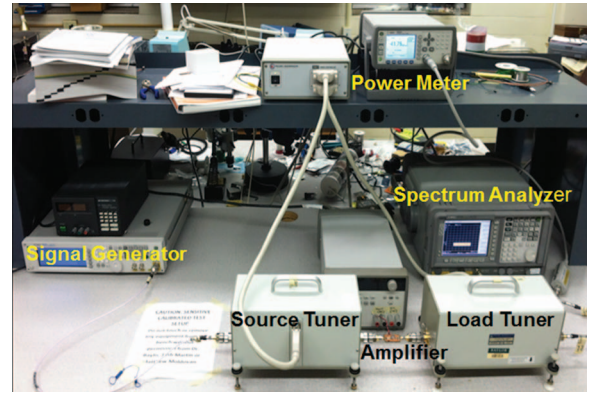


Fig. 6. Measurement setup.

change), and also allows adjustment of  $\Gamma_L$  at a value of  $B$  closer to the optimum. The number of times to run through the process of Parts A and B must be determined by the resolution required in  $\Gamma_L$  and  $B$  (i.e., how good is good enough?) and the number of queries feasible given the reconfiguration time available. In our laboratory, we have used a rule-of-thumb goal of keeping the number of experimental queries at or below 30.

For additional iterations of Parts A and B, it is often desirable to change the settings to allow faster and higher-resolution searches. For example, the step size  $D_s$  for the  $\Gamma_L$  search and the bandwidth range can be reduced when it is concluded that the search has reached the general vicinity of the solution. Fig. 3 illustrates a situation in which the search is performed twice. In the examples we have shown, the second step of the search is performed using the endpoint and reduced step values (in both  $\Gamma_L$  and  $B$ ) resulting from the first step of the search. This assumes that the results from the first iteration (Step 1) are very close to the optimum and allows subsequent steps to quickly perform fine-tuning of the results.

## IV. MEASUREMENT RESULTS

The algorithm was tested in measurement using a Skyworks amplifier on the Baylor load-pull test bench. Fig. 6 illustrates the measurement setup in the laboratory of the authors. The chirp waveform was optimized using an Agilent Technologies N5182 MXG signal generator under control of MATLAB. Tuning of the load reflection coefficient  $\Gamma_L$  was performed using the Maury Microwave Automated Tuner System load-pull software and measurement setup. A Maury MT982B 0.8–18 GHz impedance tuner was used for varying  $\Gamma_L$ . Power measurements used for PAE calculation were taken using an Agilent AT N911A power meter and Agilent AT N1921A wideband power sensor. For ACPR measurements, an Agilent E4407B 9 kHz–26.5 GHz spectrum analyzer was used. An input power of 2 dBm was used for all measurements, which placed the device approximately 2 dB into compression.

The two-step algorithm was tested. The goal of the search was to maximize the chirp bandwidth  $B$  while

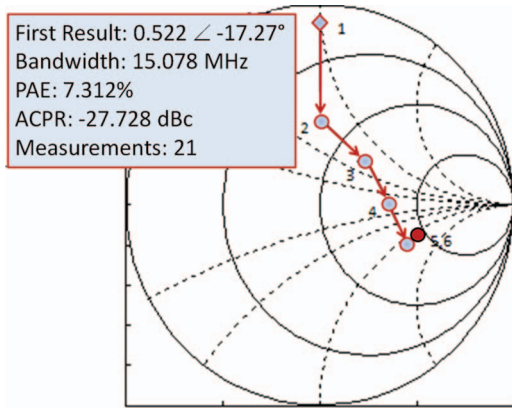


Fig. 7. Single-iteration search results for starting  $\Gamma_L = 0.9/90^\circ$  and bandwidth range of 5–20 MHz. Values of  $\Gamma_L$  and  $B$  are sought producing largest bandwidth while maintaining PAE  $\geq 7\%$  and ACPR  $\leq -27.5$  dBc. Total of 21 experimental queries were required for Step 1 (including both  $\Gamma_L$  and  $B$  parts of optimization step).

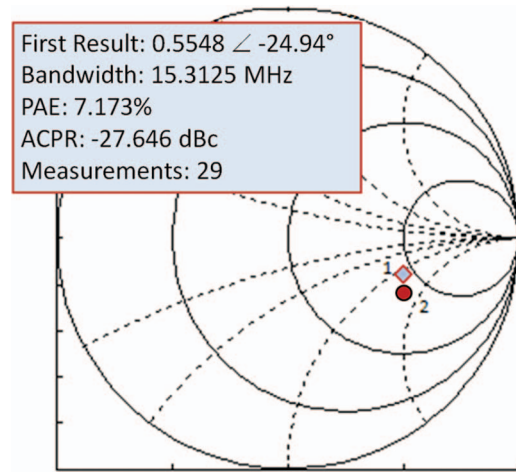


Fig. 8. Double-iteration search results for starting  $\Gamma_L = 0.9/90^\circ$  and bandwidth range of 5–20 MHz. Values of  $\Gamma_L$  and  $B$  are sought producing largest bandwidth while maintaining PAE  $\geq 7\%$  and ACPR  $\leq -27.5$  dBc. Total of 29 experimental queries were required for Steps 1 and 2 (including both  $\Gamma_L$  and  $B$  parts of each optimization step).

providing ACPR  $\leq -27.5$  dBc and PAE  $\geq 7\%$ . The parameters for the search were defined as follows:  $B_{\text{stop}} = 0.25$  MHz, PAE<sub>limit</sub> = 7.0%, and ACPR<sub>limit</sub> = -27.5 dBc.

Fig. 7 shows the results for a single iteration of the search, with starting load reflection coefficient  $\Gamma_L = 0.9e^{j90^\circ} = 0.9 / -90^\circ$  (this shorthand notation will be used to represent the exponential with an imaginary argument) and initial bandwidth search range of 5–20 MHz.

The search first found the value of  $\Gamma_L$  providing the lowest value of ACPR while maintaining PAE  $\geq 7\%$  (Part A). This is performed for the center bandwidth in the range (in this case, 12.5 MHz). The results of Part A show that the optimum ACPR value under the PAE constraint was less than the specified limit of -27.5 dBc, so the interval halving was enacted toward the upper end of the range. The value of  $\Gamma_L$  was held constant at the found optimum value of  $\Gamma_L = 0.52 / -17.3^\circ$  and the value of  $B$  was set to halve between 12.5 MHz and the upper end of the bandwidth interval, giving  $B = 16.25$  MHz. For  $B = 16.25$  MHz, the ACPR was found to be too large, so the interval between 16.25 MHz and the highest bandwidth for which the ACPR and PAE were compliant was halved, giving  $B = 14.375$  MHz. For this  $B$ , the ACPR was again found to be compliant, resulting in an interval halving between 14.375 and 16.25 MHz, or  $B = 15.3125$  MHz. The measurement at  $B = 15.3125$  MHz gave an ACPR value that was greater than the limiting value, so the interval between 14.375 and 15.3125 MHz was halved, resulting in  $B = 14.84375$  MHz. The measurement at this value of  $B$  was within ACPR and PAE compliance, resulting in an interval halving between 14.84375 and 15.3125 MHz ( $B = 15.078125$  MHz). At this value of  $B$ , the measured values of ACPR and PAE were found to be within compliance. However, the half-interval size at this point was calculated as 0.234 MHz, which is below the value of  $B_{\text{stop}}$  ( $B_{\text{stop}} = 0.25$  MHz). The search was thus terminated and the value of  $B = 15.078$  MHz was identified as the maximum chirp bandwidth, while the optimum

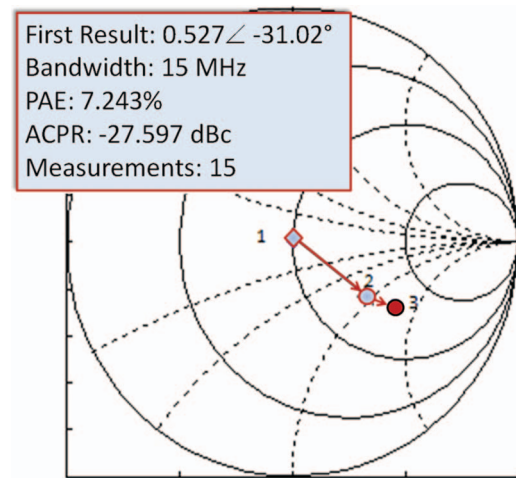


Fig. 9. Single-iteration search results for starting  $\Gamma_L = 0$  and bandwidth range of 12–20 MHz. Values of  $\Gamma_L$  and  $B$  are sought producing largest bandwidth while maintaining PAE  $\geq 7\%$  and ACPR  $\leq -27.5$  dBc. Total of 15 experimental queries were required for Step 1 (including both  $\Gamma_L$  and  $B$  parts of optimization step).

reflection coefficient was identified as  $\Gamma_L = 0.52 / -17.3^\circ$ . For the single-iteration search, the final values of PAE and ACPR were PAE = 7.31% and ACPR = -27.7 dBc.

A second major iteration of the search (Step 2) was then performed to examine the benefits of reoptimizing for  $\Gamma_L$  and then reoptimizing for  $B$ . Fig. 8 shows the results of the reoptimization. Slight changes are found in the identified optimum values of  $\Gamma_L = 0.55 / -31.9^\circ$  and  $B = 15.3125$  MHz. As expected, a fine-tuning was performed for a slight bandwidth increase, at the expense of eight additional measurements.

While Figs. 7 and 8 show the results of one and two major iterations, respectively, for a starting reflection coefficient  $\Gamma_L = 0.9 / -90^\circ$  and bandwidth range of 5–20 MHz, Figs. 9 and 10 show a comparison from different starting conditions:  $\Gamma_L = 0$  and bandwidth range

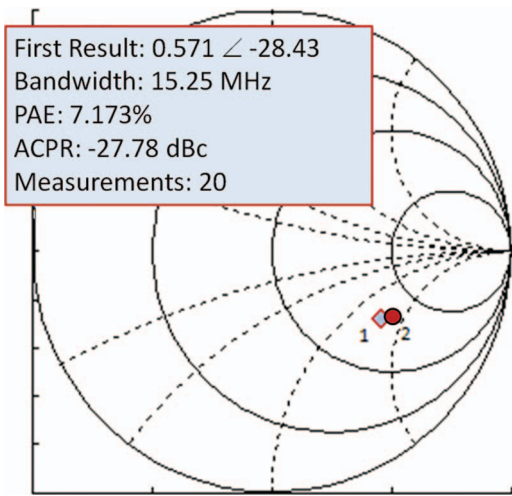


Fig. 10. Double-iteration search results for starting  $\Gamma_L = 0$  and bandwidth range of 12–20 MHz. Values of  $\Gamma_L$  and  $B$  are sought producing largest bandwidth while maintaining  $\text{PAE} \geq 7\%$  and  $\text{ACPR} \leq -27.5$  dBc. Total of 20 experimental queries were required for Steps 1 and 2 (including both  $\Gamma_L$  and  $B$  parts of each optimization step).

of 12–20 MHz. Fig. 9 shows the results of a single-iteration search from these conditions. The first stage, the search for  $\Gamma_L$  providing the lowest ACPR possible with  $\text{PAE} \geq 7\%$ , was completed with a mere 11 measurements at the center bandwidth value of 16 MHz. A value of  $\Gamma_L = 0.53 \angle -31.0^\circ$  was found to be the optimum reflection coefficient, but this reflection coefficient resulted in an ACPR greater than the specified maximum of  $-27.5$  dBc. Because a smaller bandwidth interval was specified than the search displayed in Fig. 7, the bandwidth-adjustment part of the search was expected to complete more quickly, and this was indeed found to be the case.

In Step B of the search, the first measurement was performed at  $B = 14$  MHz. Unlike the 16 MHz measurement, this measurement passed both the ACPR and PAE requirements. A measurement was then performed for  $B = 15$  MHz, which also passed. The measurement for  $B = 15.5$  MHz failed ACPR requirements. Finally, the measurement for  $B = 15.25$  MHz failed requirements. For interval halving to be performed again, the bandwidth step would be 0.125 MHz, below the specified search parameter  $B_{\text{stop}} = 0.25$  MHz. The search thus stopped, specifying  $\Gamma_L = 0.53 \angle -31.0^\circ$  and  $B = 15$  MHz as the optimum combination of reflection coefficient and bandwidth. This combination was found with only 15 total measurements. The final PAE and ACPR values were measured as 7.24% and  $-27.6$  dBc. It appears that some margin exists between the measured PAE value and the limit of 7%. This raises the question of whether additional bandwidth can be gained in some cases by a second iteration of the search (with decrease of PAE).

Indeed, slightly higher bandwidth was obtained by extending the search to a second iteration. The results are

shown in Fig. 10. It can be seen that the optimal value of  $\Gamma_L$  changed slightly from its first-iteration endpoint, to  $0.57 \angle -28.4^\circ$ . This change provided a larger bandwidth value of 15.25 MHz, to be obtained in the next interval-halving step. The resultant PAE (7.17%) and ACPR ( $-27.6$  dBc) values are slightly closer to the boundaries of 7% and  $-27.5$  dBc. These results indicate that a sacrifice was made (especially in PAE) to increase the bandwidth while still remaining within requirements. For a total of five additional measurements required, an additional 250 kHz of chirp bandwidth was obtained.

Single- and double-iteration searches were attempted for multiple starting  $\Gamma_L$  values and bandwidth ranges. The results for the multiple starting points for a single iteration are shown in Table I. Results for two iterations (the first iteration as detailed by the Table I results, followed by a second iteration starting at the endpoint of the first iteration) are shown in Table II. Two of the searches used the starting load reflection coefficient that was found previously to provide maximum PAE for  $B = 16$  MHz:  $\Gamma_L = 0.44 \angle -19.5^\circ$ .

The results of Table I show that the values of load reflection coefficient  $\Gamma_L$  and final chirp bandwidth  $B$  are very similar across multiple starting reflection coefficient values and bandwidth search ranges. The resolution of the bandwidth discernment in the search is related to the  $B_{\text{stop}}$  parameter. Accordingly,  $B_{\text{stop}}$  gives a measure of the expected correspondence and deviation of the final  $B$  values selected by the search. The PAE and ACPR values of the endpoints are close to their respective limits (7% for PAE and  $-27.5$  dBc for ACPR) but meet the requirements, and the final chirp bandwidth  $B$  is approximately 15 MHz in all cases. The number of measurements for a single-iteration search varies from 13 to 24 across all experiments. This algorithm seems to use a small number of measurements, considering that both the circuitry and waveform bandwidth are optimized.

For the double-iteration search, the difference between end  $\Gamma_L$  values is much smaller, and a larger bandwidth appears to be found, on average. We suspect that this is because the second iteration provides for adjustment for any variation of the PAE with increasing bandwidth, allowing the PAE and ACPR to be pushed closer to limitations to try to obtain more bandwidth. Of course, the number of times the search is repeated can be determined by the user. The user must weigh the benefit of added resolution (and potentially more bandwidth) against the number of additional experimental queries necessary to obtain the improvement. It appears in many of the cases shown that the second iteration, while requiring five to eight extra measurements, produces only minimal improvement. For certain devices and circumstances, the cost in additional reconfiguration time may not be worth obtaining this minimal improvement, especially in a real-time reconfigurable radar that is changing on the fly.

TABLE I  
Single-Iteration Algorithm Results

Start $\Gamma_L$	Bandwidth Range (MHz)	End $\Gamma_L$	ACPR (dBc)	PAE (%)	Final Chirp Bandwidth $B$ (MHz)	Number of Measurements
0.44 / $-19.5^\circ$	5–20	0.49 / $-17.6^\circ$	-27.6	7.39	14.84	13
0.9 / $90^\circ$	5–20	0.52 / $-17.3^\circ$	-27.7	7.31	15.08	21
0	12–20	0.53 / $-31.0^\circ$	-27.6	7.24	15.00	15
0.9 / $180^\circ$	12–20	0.52 / $-36.8^\circ$	-27.5	7.12	15.25	24
0.44 / $-19.5^\circ$	10–20	0.49 / $-17.6^\circ$	-27.9	7.23	15.00	13
0.9 / $-90^\circ$	10–20	0.54 / $-26.2^\circ$	-27.6	7.23	15.31	18
0	15–20	0.55 / $-31.9^\circ$	-27.6	7.10	15.31	17
0.9 / $0^\circ$	15–20	0.55 / $-9.9^\circ$	-27.6	7.13	15.31	14

Note: ACPR = alternate-channel power ratio. PAE = power-added efficiency.

TABLE II  
Double-Iteration Algorithm Results

Start $\Gamma_L$	Bandwidth Range (MHz)	End $\Gamma_L$	ACPR (dBc)	PAE (%)	Final Chirp Bandwidth $B$ (MHz)	Number of Measurements
0.44 / $-19.5^\circ$	5–20	0.54 / $-16.0^\circ$	-27.5	7.22	15.31	18
0.9 / $90^\circ$	5–20	0.55 / $-24.9^\circ$	-27.6	7.17	15.31	29
0	12–20	0.57 / $-28.4^\circ$	-27.8	7.09	15.25	20
0.9 / $180^\circ$	12–20	0.52 / $-36.8^\circ$	-27.5	7.12	15.25	29
0.44 / $-19.5^\circ$	10–20	0.54 / $-16.0^\circ$	-27.6	7.15	15.31	18
0.9 / $-90^\circ$	10–20	0.55 / $-28.5^\circ$	-27.5	7.15	15.47	23
0	15–20	0.55 / $-31.9^\circ$	-27.6	7.10	15.31	22
0.9 / $0^\circ$	15–20	0.57 / $-17.5^\circ$	-27.5	7.11	15.47	22

Note: ACPR = alternate-channel power ratio. PAE = power-added efficiency.

## V. CONCLUSIONS

This article has demonstrated a method for intelligently optimizing load reflection coefficient and input waveform bandwidth to maximize the bandwidth while meeting requirements for adjacent-channel power ratio and power-added efficiency. This algorithm is expected to find useful application in optimizing range resolution of adaptive radars while ensuring high-efficiency performance and spectral compliance. Results have been demonstrated using measurements with a setup containing a signal generator capable of generating chirp waveforms of different bandwidths and a microwave load-pull tuner system. In the experiment detailed in the article, convergence of bandwidth and load reflection coefficient to very similar values was found for a test amplifier by using between 13 and 24 measured data points. The ability to reconfigure quickly shows excellent promise for integrating this algorithm in future real-time reconfigurable radar transmitters.

## ACKNOWLEDGMENT

The authors are appreciative to program manager Dr. George Haddad for his support of this work.

## REFERENCES

- [1] Fellows, M., Baylis, C., Martin, J., Cohen, L., and Marks, R. J., II. Direct algorithm for the Pareto load-pull optimisation of power-added efficiency and adjacent-channel power ratio. *IET Radar, Sonar & Navigation*, **8**, 9 (Dec. 2014), 1280–1287.
- [2] Sevic, J. F., Burger, K. L., and Steer, M. B. A novel envelope-termination load-pull method for ACPR optimization of RF/microwave power amplifiers. In *1998 IEEE MTT-S International Microwave Symposium Digest*, Baltimore, MD, June 1998, **2**, 723–726.
- [3] Sevic, J. F., Steer, M. B., and Pavio, A. M. Large-signal automated load-pull of adjacent-channel power ratio for digital wireless communication systems. In *1996 IEEE MTT-S International Microwave Symposium Digest*, San Francisco, CA, June 1996, **2**, 763–766.
- [4] Fellows, M., Flachsbarth, M., Barlow, J., Baylis, C., and Marks, R. J., II. The Smith Tube: Selection of radar chirp waveform bandwidth and power amplifier load impedance using multiple-bandwidth load-pull measurements. In *2014 IEEE 15th Annual Wireless and Microwave Technology Conference*, Tampa, FL, June 2014.
- [5] Wu, Q., Xiao, H., and Li, F. Linear RF power amplifier design for CDMA signals: A spectrum analysis approach. *Microwave Journal*, **41** (1998).
- [6] Sechi, F. N. Design procedure for high-efficiency linear microwave power amplifiers. *IEEE Transactions on Microwave Theory and Techniques*, **MTT-28**, Pt. 1 (Nov. 1980), 1157–1163.
- [7] Sun, Y., and Lau, W. K. Evolutionary tuning method for automatic impedance matching in communication systems. In *1998 IEEE International Conference on Electronics, Circuits and Systems*, Lisboa, Portugal, Sept. 1998, **3**, 73–77.
- [8] Sun, Y., and Lau, W. K. Antenna impedance matching using genetic algorithms.

- In *IEEE National Conference on Antennas and Propagation*, York, United Kingdom, Mar.–Apr. 1999, 31–36.
- [9] Arroyo-Huerta, E., Diaz-Mendez, A., Ramirez-Cortes, J. M., and Garcia, J. C. S.  
An adaptive impedance matching approach based on fuzzy control.  
In *52nd IEEE International Midwest Symposium on Circuits and Systems*, Cancún, Mexico, Aug. 2009, 889–892.
- [10] Hemminger, T. L.  
Antenna impedance matching with neural networks.  
*International Journal of Neural Systems*, **15**, 5 (Oct. 2005), 357–361.
- [11] Munshi, A. S., Johns, D. A., and Sedra, A. S.  
Adaptive impedance matching.  
In *1994 IEEE International Symposium on Circuits and Systems*, London, United Kingdom, May–June 1994, 2, 69–72.
- [12] Sun, Y., Moritz, J., and Zhu, X.  
Adaptive impedance matching and antenna tuning for green software-defined and cognitive radio.  
In *2011 IEEE 54th International Midwest Symposium on Circuits and Systems*, Seoul, South Korea, Aug. 2011.
- [13] Kingsley, N., and Guerci, J. R.  
Adaptive amplifier module technique to support cognitive RF architectures.  
In *2014 IEEE Radar Conference*, Cincinnati, OH, May 2014, 1329–1332.
- [14] Haykin, S.  
Cognitive radar: A way of the future.  
*IEEE Signal Processing Magazine*, **23**, 1 (Jan. 2006), 30–40.
- [15] Guerci, J. R.  
*Cognitive Radar: The Knowledge-Aided Fully Adaptive Approach*. Norwood, MA: ArtechHouse, 2010.
- [16] Chen, R., and Cantrell, B.  
Highly bandlimited radar signals.  
In *Proceedings of the IEEE Radar Conference*, Long Beach, CA, Apr. 2002, 220–226.
- [17] Blunt, S., Cook, M., Perrins, E., and de Graaf, J.  
CPM-based radar waveforms for efficiently bandlimiting a transmitted spectrum.  
In *2009 IEEE Radar Conference*, Pasadena, CA, May 2009.
- [18] Cook, M. R.  
CPM-based radar waveforms for efficiently bandlimiting a transmitted spectrum.  
M.S. thesis, University of Kansas, Lawrence, 2010.
- [19] Moldovan, M., Baylis, C., Wicks, M., Martin, J., and Marks, R. J., II.  
Chirp optimization using piecewise linear approach.  
In *2012 International Diversity & Design Conference*, Kauai, HI, January 2012.
- [20] Fellows, M., Baylis, C., Cohen, L., and Marks, R. J., II.  
Radar waveform optimization to minimize spectral spreading and achieve target detection.  
In *2013 Texas Symposium on Wireless and Microwave Circuits and Systems*, Waco, TX, Apr. 2013.
- [21] Patton, L. K.  
On the satisfaction of modulus and ambiguity function constraints in radar waveform optimization for detection.  
Ph.D. dissertation, Wright State University, Dayton, OH, 2007.
- [22] Holtzman, J., and Thorp, J. S.  
Optimum signals for radar.  
*IEEE Transactions on Aerospace and Electronic Systems*, **AES-5**, 6 (Nov. 1969), 898–905.
- [23] Wong, K. T., and Chung, W.-K.  
Pulse-diverse radar/sonar FSK-PSK waveform design to emphasize/de-emphasize designated Doppler-delay sectors.  
In *The Record of the IEEE 2000 International Radar Conference*, Alexandria, VA, May 2000, 745–749.
- [24] Sussman, S.  
Least-square synthesis of radar ambiguity functions.  
*IRE Transactions on Information Theory*, **8**, 3 (Apr. 1962), 246–254.
- [25] Guerci, J. R., and Pillai, S. U.  
Adaptive transmission radar: The next “wave”?  
In *Proceedings of the 2000 IEEE National Aerospace and Electronics Conference*, Dayton, OH, Oct. 2000, 779–786.
- [26] Haykin, S., Xue, Y., and Davidson, T. N.  
Optimal waveform design for cognitive radar.  
In *42nd Asilomar Conference on Signals, Systems and Computers*, Pacific Grove, CA, Oct. 2008, 3–7.
- [27] Goodman, N. A., Venkata, P. R., and Neifield, M. A.  
Adaptive waveform design and sequential hypothesis testing for target recognition with active sensors.  
*IEEE Journal of Selected Topics in Signal Processing*, **1**, 1 (June 2007), 105–113.
- [28] Jakabosky, J., Blunt, S. D., Cook, M. R., Stiles, J., and Seguin, S. A.  
Transmitter-in-the-loop optimization of physical radar emissions.  
In *2012 IEEE Radar Conference*, Atlanta, GA, May 2012, 874–879.
- [29] Raab, F. H., Asbeck, P., Cripps, S., Kenington, P. B., Popovic, Z. B., Potheary, N., Sevic, J. F., and Sokal, N. O.  
Power amplifiers and transmitters for RF and microwave.  
*IEEE Transactions on Microwave Theory and Techniques*, **50**, 3 (Mar. 2002), 814–826.
- [30] Zelle, C.  
A spherical representation of the Smith chart.  
*IEEE Microwave Magazine*, **8**, 3 (June 2007), 60–66.
- [31] Wu, Y., Zhang, Y., Liu, Y., and Huang, H.  
Theory of the spherical generalized Smith chart.  
*Microwave and Optical Technology Letters*, **51**, 1 (Jan. 2009), 95–97.
- [32] Shamim, A., Radwan, A. G., and Salama, K. N.  
Fractional Smith chart theory.  
*IEEE Microwave and Wireless Components Letters*, **21**, 3 (Mar. 2011), 117–119.
- [33] Kretzschmar, J., and Schoonaert, D.  
Smith chart for lossy transmission lines.  
*Proceedings of the IEEE*, **57**, 9 (Sept. 1969), 1658–1660.
- [34] Geis, L. A., and Dunleavy, L. P.  
Power contour plots using linear simulators.  
*Microwave Journal*, **39**, 6 (1996), 60–71.
- [35] Hajji, R., Beauregard, F., and Ghannouchi, F. M.  
Multitone power and intermodulation load-pull characterization of microwave transistors suitable for linear SSPA’s design.  
*IEEE Transactions on Microwave Theory and Techniques*, **45**, 7 (July 1997), 1093–1099.
- [36] Pozar, D. M.  
*Microwave Engineering*, 4th ed. Hoboken, NJ: John Wiley & Sons, 2012.
- [37] Martin, J., Baylis, C., Cohen, L., de Graaf, J., and Marks, R. J., II.  
A peak-search algorithm for load-pull optimization of power-added efficiency and adjacent-channel power ratio.  
*IEEE Transactions on Microwave Theory and Techniques*, **62**, 8 (Aug. 2014), 1772–1783.

**Matthew Fellows** completed his bachelor and master of science degrees in electrical and computer engineering at Baylor University in 2012 and 2014, respectively. He is currently pursuing his Ph.D. degree at Baylor. His research is focusing on the creation of algorithms for the joint optimization of radar-transmitter power-amplifier circuitry and waveforms. He has published several articles related to his areas of interest.

**Matthew Flachsbart** is a student at Baylor University, where he plans to complete his bachelor of science degree in electrical and computer engineering in 2015. His research focuses on the development and implementation of algorithms for circuit optimizations.

**Jennifer Barlow** is a student at Baylor University, where she plans to complete her bachelor of science degree in electrical and computer engineering in 2015. Her research focuses on intelligent load-pull measurements for optimizable power amplifiers.

**Joseph Barkate** received his bachelor of science degree in electrical and computer engineering from Baylor University in 2014. He is currently working toward a master of science degree in electrical and computer engineering and is focusing his research on intelligently optimizable power amplifiers.



**Charles Baylis** (S'03–M'08) is an associate professor of electrical and computer engineering at Baylor University, where he directs the Wireless and Microwave Circuits and Systems Program. Dr. Baylis received B.S., M.S., and Ph.D. degrees in electrical engineering from the University of South Florida in 2002, 2004, and 2007, respectively. His research focuses on spectrum issues in radar and communication systems and has been sponsored by the National Science Foundation and the Naval Research Laboratory. He has focused his work on the application of microwave circuit technology and measurements, combined with intelligent optimization algorithms, to creating reconfigurable transmitters. He serves as the general chair of the annual Texas Symposium on Wireless and Microwave Circuits and Systems, technically cosponsored by the IEEE Microwave Theory and Techniques Society (MTT-S). He also serves as student activities chair of the IEEE MTT-S Dallas chapter.

**Lawrence Cohen** (M'87–SM'12) has been involved in electromagnetic compatibility (EMC) engineering and management, shipboard antenna integration, and radar system design for 33 years. In this capacity he has worked in the areas of shipboard electromagnetic interference problem identification, quantification and resolution, mode-stirred chamber research, and radar absorption material design, test, and integration. In March of 2007, Mr. Cohen acted as the Navy's principal investigator in the assessment of radar emissions on a WiMAX network. Additionally, he has acted as the principal investigator for various radar programs, including the radar transmitter upgrades. Currently, he is involved with identifying and solving spectrum conflicts between radar and wireless systems, as well as research into spectrally cleaner power-amplifier designs, tube and solid state.

Mr. Cohen received a bachelor of science degree in electrical engineering from the George Washington University in 1975 and a master of science degree in electrical engineering from Virginia Tech in 1994. He is certified as an EMC engineer by the National Association of Radio and Telecommunications Engineers. He served as the technical program chairman for the IEEE 2000 International Symposium on EMC and was elected for three-year terms to the IEEE EMC Society Board of Directors in 1999 and 2009. He is also a member of the IEEE EMC Society Technical Committee 6 for Spectrum Management. For the past 26 years he has been employed by the Naval Research Laboratory in Washington, DC. In his spare time he enjoys golf, hiking, cycling, and target shooting.



**Robert J. Marks, II** (S'71–M'72–SM'83–F'94), is a distinguished professor of electrical and computer engineering at Baylor University, Waco, Texas. When at the University of Washington, he served for 17 years as the faculty advisor to the student chapter of Campus Crusade for Christ. He is a Fellow of IEEE and the Optical Society of America. His most recent books are *Handbook of Fourier Analysis and Its Applications* (Oxford University Press, 2009) and *Biological Information—New Perspectives* (Singapore: World Scientific, 2013), coedited by M. J. Behe, W. A. Dembski, B. L. Gordon, and J. C. Sanford. He has an Erdős–Bacon number of 5.